Intermediate-Sized Conjugated Donor Molecules for Organic Solar Cells: Comparison of Benzodithiophene and Benzobis-thiazole-based Cores.

Siyuan Zhang,[†,¶] Junxiang Zhang,[†,¶] Maged Abdelsamie,[‡] Qinqin Shi,[§] Yadong Zhang,[†] Timothy C. Parker,[†] Evgheni V. Jucov,[||] Tatiana V. Timofeeva,[||] Aram Amassian,[‡] Guillermo C. Bazan,[∫] Simon B. Blakey,[§] Stephen Barlow,[†] Seth R. Marder*[,†].

[†]Center for Organic Photonics and Electronics and School of Chemistry and Biochemistry Georgia Institute of Technology, Atlanta, GA 30332-0400, United States

[‡]Division of Physical Sciences and Engineering Solar and Photovoltaic Engineering Research Center (SPERC), King Abdullah University of Science and Technology (KAUST), Thuwal, 23955–6900, Saudi Arabia

[§]Department of Chemistry, Emory University, Atlanta, GA 30322, United States

[||]Department of Chemistry, New Mexico Highlands University, Las Vegas, NM 87701, United States

[∫]Center for Polymers and Organic Solids, Department of Chemistry and Biochemistry, and Department of Physics, University of California, Santa Barbara, CA 93106, United States

ABSTRACT: Two intermediate-sized donor molecules, **BBTz-X** and **BDT-X**, have been synthesized by the Stille coupling between 4-(4,4-bis(2-ethylhexyl)-6-(trimethylstannyl)-4*H*-silolo[3,2-*b*:4,5-*b*′]dithiophen-2-yl)-7-(5'-hexyl-[2,2'-bithiophen]-5-yl)-[1,2,5]thiadiazolo[3,4-*c*]pyridine and either 4,8-bis(5-(2-ethylhexyl)thiophen-2-yl)-2,6-diiodobenzo[1,2-*d*:4,5-*d*′]bis(thiazole) or 2,6-dibromo-4,8-bis(5-(2-ethylhexyl)thiophen-2-yl)benzo[1,2-*b*:4,5-*b*′]dithiophene, respectively. Both oxidation and reduction potentials for **BBTz-X** are anodically shifted relative to those for **BDT-X**, but the oxidation potential is more sensitive to the identity of the core; this is consistent with what is seen for DFT-calculated HOMO and LUMO energies and with a slightly blue-shifted absorption maximum for **BBTz-X**. Although DFT calculations, along with crystal structures of related compounds, suggest more planar molecular structures for **BBTz-X** than for **BDT-X**, film structures and the effects of various annealing processes on these films, as revealed by GIWAXS are similar. The performance of **BDT-X**:$PC_{61}BM$ bulk-heterojunction solar cells is more sensitive to annealing conditions than that of **BBTz-X**:$PC_{61}BM$ cells, but, under appropriate conditions, both yield power conversion efficiencies of >7%.

INTRODUCTION

Light-harvesting materials for organic solar cells (OSCs) frequently incorporate molecular electron donor (D) and electron acceptor (A) building blocks in an alternating and conjugated manner in order to achieve high absorption coefficients in the low-energy region of solar spectrum. Variation of the D and A moieties allows the absorption energy, ionization energy (IE), and electron affinity (EA) to be changed to obtain the desired material properties for devices. This D-A concept has been widely applied to both conjugated polymers and to small molecules, and to both hole- and electron-transporting materials.[1-10] In the past few years, power conversion efficiencies (PCEs) of >11% and >13% have been achieved for bulk heterojunction (BHJ) cells consisting of hole-transporting D-A polymers as donors in combination with fullerene[11] and non-fullerene acceptors, respectively.[12] BHJ cells based on solution-processable hole-transporting small molecules have exhibited PCEs of ca. 10% in combination with either fullerenes[13,14] or non-fullerenes.[15] Advantages of small molecules over their polymeric counterparts include their good solubility, often high open-circuit voltages (V_{oc}),[16] and their well-defined chemical structures, which can alleviate issues associated with batch-to-batch variability of molecular-weight distribution in polymers.[17-21] However, often they exhibit poorer film quality, lower J_{sc}, and less thermally stable phases in the solid state.[16,22]

Recently, several "oligomers" or "intermediate"-sized (*i.e.*, non-polymeric) OSC donors, consisting of 6-10 rings, have been synthesized with the aim of combining some of the desirable qualities of polymer and small-molecule classes.[23-26] The Bazan group reported a series of intermediate-sized conjugated molecules of the general type represented by Figure 1, i.e. D^1–A–D^2–core–D^2–A–D^1 structures, with D^1 and D^2 representing 5'-hexyl-(2,2'-bithiophen)-5-yl (BiTh) and dithieno(3,2-*b*;2',3'-*d*)silole-2,6-diyl (DTS) moieties, respectively, and A being pyridal[2,1,3]thiadiazole (PT).[21,23] By varying the center

"core", the optical properties, IE and EA, thermal stability, charge-carrier mobilities, microstructural characteristics, and OSC performance were adjusted. One of the most efficient molecules in this type was **X2** (Figure 1); BHJ OSCs with $PC_{61}BM$ and $PC_{71}BM$ exhibited PCE values of 6.4% and 7.4% in a conventional indium tin oxide (ITO)/MoO_x/active layer/Al device structure.[23,27]

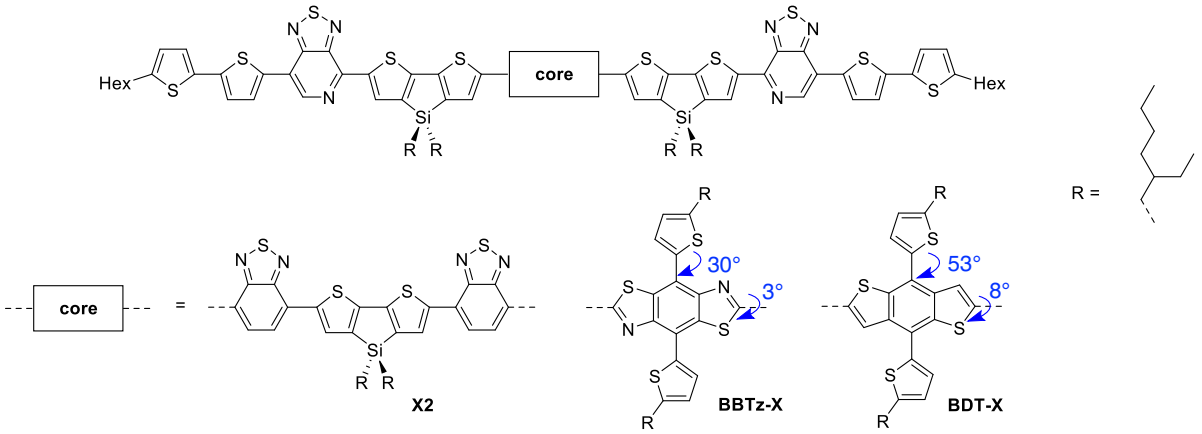

Figure 1. Chemical structures of intermediate-sized molecules with various core units: **X2** (previously reported by Bazan *et al.*)[23] and new compounds **BBTz-X** and **BDT-X** used in this study (angles are from B3LYP/6-311G* calculations).

Benzo[1,2-*b*:4,5-*b*']dithiophene (BDT) derivatives are well-established building blocks for both polymeric and molecular OSC hole-transporting light-harvesting materials,[15,18,22,24,25,28-38] some of which have afforded PCE values of over 12%.[37,38] Benzo[1,2-*d*:4,5-*d*']bisthiazole (BBTz) derivatives have also been incorporated into OPV materials,[39-41] but have received much less attention than their BDT analogues, presumably, at least in part, due to the challenges associated with their functionalization; the BBTz core is unstable to strongly basic conditions, such as lithiation conditions,[42] commonly required for the synthesis of stannyl or boryl derivatives; additionally, the electron-poor nature of BBTz renders it resistant to electrophilic halogenation. Although 2,6-dibromo-4,8-di(2-ethylhexyloxy)benzo[1,2-*d*:4,5-*d*']bis(thiazole) has been obtained through the Sandmeyer reaction of the corresponding 2,6-diamino compound, itself obtained by the Hantzsch-type cyclization of bromoanilic acid with thiourea,[37] the intermediates were reported to be unstable and the overall yield was low. However, recently arylation[43] and iodination[44] of the 2,6-positions of BBTz have been reported using C-H functionalization and a ^{t}BuOK-initiated reaction with C_6F_5I, respectively.

Here we report the synthesis, characterization, and OSC performance of two new intermediate-sized molecules, **BDT-X** and **BBTz-X**, in which the "arms" of **X2** are attached to 2,6-positions of 4,8-di(5-alkylthiophen-2-yl)-substituted benzo[1,2-*b*:4,5-*b*']dithiophene (BDT) and benzo[1,2-*d*:4,5-*d*']bisthiazole (BBTz) core moieties (Figure 1a). The 4,8 substituents were chosen since it has been suggested that inclusion of thienyl or aryl groups in these positions impart "2D character" to the frontier orbitals, leading to more pathways for interchain π-overlap and consequently improved exciton diffusion and/or charge transport in such materials.[45,46] Different film processing methods and post-deposition treatments were used to examine how variation of the core segment influences the solid-state order, and hence the electrical and photovoltaic properties. BHJ OSCs using $PC_{61}BM$ achieved PCE >7% with either donor molecule, higher than that obtained using **X2** as the donor in devices fabricated under the same conditions.

RESULTS AND DISCUSSION

Synthesis and Characterization. As discussed above, recently developed direct arylation[43] and iodination[44] methods facilitate the incorporation of BBTz into π-conjugated systems. Although useful, the former approach may not be sufficiently effective for coupling with substrates that contain multiple C–H bonds susceptible to the direct arylation conditions. Accordingly, 4,8-bis(5-(2-ethylhexyl)thiophen-2-yl)-2,6-diiodobenzo[1,2-*d*:4,5-*d*']bis(thiazole) was synthesized using the same iodination conditions previously applied to its 4,8-bis(5-(2-ethylhexyl)-4-hexylthiophen-2-yl) analogue,[44] and subsequently converted to **BBTz-X** by coupling with two equivalents of stannylated "X" side-arm.[23,47] using Stille conditions similar to those previously used to synthesize **X2**.[23,47] 4,8-Bis(5-(2-ethylhexyl)thiophen-2-yl)-2,6-dibromobenzo[1,2-*b*:4,5-*b*']dithiophene[48] was used in an analogous coupling to obtain **BDT-X**. The structures and purities of **BBTz-X** and **BDT-X** were confirmed by NMR spectroscopy, mass spectrometry and elemental analysis. Experimental details and characterizing data are given in the Supporting Information (SI).

The thermal properties of **BDT-X** and **BBTz-X** were investigated by thermogravimetric analysis (TGA, 10 °C min^{-1}) and differential scanning calorimetry (DSC, 10 °C min^{-1}) under nitrogen (Figure S1). TGA decomposition temperatures (5% weight loss) are 439 and 406 °C for **BBTz-X** and **BDT-X**, respectively. DSC (Figure 2a, second heating; similar behavior is seen on the third heating/cooling cycle as shown in Figure S2 in the SI) indicates endothermic transitions attributable to melting at 256 and 215 °C for **BBTz-X** and **BDT-X**, respectively, with

corresponding exothermic crystallization peaks seen on cooling at 225 and 198 °C, respectively. In addition, **BBTz-X** shows an transition with a lower enthalpic feature (215 and 195 °C on heating and cooling respectively), possibly due to a crystal-crystal transition. The higher melting point seen for **BBTz-X** may reflect stronger intermolecular interactions for this compound. This is also consistent with the lower solubility found for **BBTz-X** in solvents including THF, CH_2Cl_2, and chlorobenzene (ca. 3 mg mL^{-1} in chlorobenzene vs. 15 mg mL^{-1} for **BDT-X**).

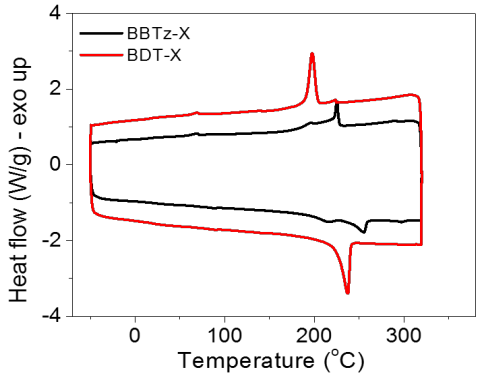

Figure 2. DSC thermograms (second heating and cooling, 10 °C min^{-1}) of **BBTz-X** and **BDT-X**.

Optical and Electronic Properties. Figure 3 shows normalized optical absorption spectra of **BBTz-X** and **BDT-X** in dilute (ca. 1×10^{-5} M) chloroform solution, and as thin films on glass slides; data are compared to **X2** in Table 1. Similar spectra are seen for the two molecules: two high-energy bands in the 350-500 nm range, and a low-energy band with higher absorptivity in the 550-750 nm range. The strong low-energy bands are, in both cases, blue-shifted from that of **X2**, with substitution of CH with N leading to a slightly greater blue shift (Table 1); similar absorptivities are seen for the low-energy bands of all three molecules. As was the case for **X2**,[23] absorption spectra of **BBTz-X** and **BDT-X** thin films are red-shifted relative to those in solution. Electrochemical redox potentials from cyclic voltammograms are also summarized in Table 1. Both the half-wave reduction and oxidation potentials of **BBTz-X** are cathodically shifted relative to those of **BBT-X** (by ca. 50 and 100 mV, respectively), consistent with the increased electron affinity and ionization energy expected on replacing CH moieties with more electronegative N atoms. The separation between the oxidation and reduction potentials of **BBTz-X** is somewhat larger for that for **BDT-X**, which in turn is larger than that of **X2**, agreeing with the trends seen in absorption maxima and onsets.

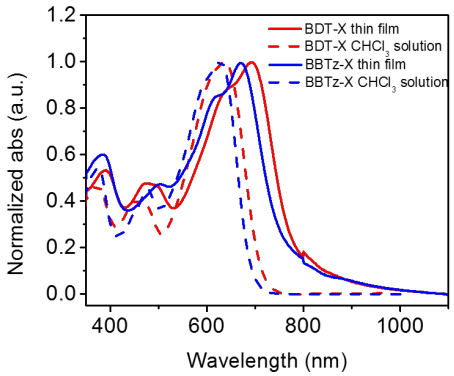

Figure 3. Normalized optical absorption spectra of compounds **BBTZ-X** and **BDT-X** in $CHCl_3$ solutions and as thin films.

Table 1. Optical and Electrochemical data, Along with Calculated Orbital Energies, for BBTz-X, BDT-X, and X2.[a]

	Optical Data			Electrochemical Data[b]			DFT Orbital Energies[c]		
	λ_{max}^{sol} / nm ($\log[\varepsilon_{max} / M^{-1} cm^{-1}]$)[d]	λ_{max}^{film} / nm	E_{gap}^{opt} / eV[e]	$E_{1/2}^{+/o}$ / V	$E_{1/2}^{o/-}$ / V	E_{gap}^{echem} / eV[f]	E_{HOMO} / eV	E_{LUMO} / eV	$E_{gap}^{orbital}$ / eV[g]
BBTz-X	477 (4.75), 626 (5.10)	668	1.63	+0.45	−1.41	1.86	−4.82	−3.02	1.80
BDT-X	452 (4.70), 631 (5.08)	692	1.59	+0.35	−1.46	1.81	−4.67	−2.94	1.73
X2	380 (4.70), 672 (5.15)	758	1.45	+0.25	−1.44	1.69	−4.88	−3.24	1.64

[a]Data for **X2** are taken from tables, or estimated from figures showing spectra and electrochemical data, in ref. 14. [b]Half-wave potentials vs. $FeCp_2^{+/o}$ in 0.1 M $^nBu_4NPF_6$ / CH_2Cl_2. [c]For isolated molecules at the B3LYP6-311G* level. [d]$CHCl_3$. [e]Estimated as the energy corresponding to the intersection with the wavelength axis of a tangent to the steepest part of the low-energy side of the lowest energy peak of the absorption spectrum of a film. [f]$E_{gap}^{echem} = e\,(E_{1/2}^{+/o} - E_{1/2}^{o/-})$. [g]$E_{gap}^{orbital} = E_{LUMO} - E_{HOMO}$.

Molecular Geometries and Orbital Energies. We have determined the X-ray crystallographic structure of a single crystal of 4,8-bis(5-(2-ethylhexyl)thiophen-2-yl)benzo[1,2-d:4,5-d']bis(thiazole), the precursor to **BBTz-X**, (Figure 4; see also SI for more discussion of the structure); angles of 11° are found between the plane of each thienyl ring and that of the BBTz core. The corresponding angles in the crystal structure of a molecule with a 4,8-di(4,5-dialkylthiophen-2-yl)-BDT core are 45 and 52°.[14] The difference in these angles can be attributed to both the reduced inter-ring steric interactions when CH is replaced with N atom, and to attractive intramolecular inter-ring $S_{thienyl}\cdots N_{thiazole}$ interactions;[49-53] the S–N distance in this structure is 2.824 Å, whereas the sum of Van der Waals radii is 3.35 Å.[53]

Density functional theory (DFT) calculations (B3LYP/6-311G*) were also used to gain insight into the molecular geometries of **BBTz-X** and **BDTz-X**. As indicated in Figure 1 and Figure S3(c), the energy-minimized dihedral angle between planes of thienyl substituents and the BDT core of **BDT-X** is ca. 53°, much larger than the calculated dihedral angle between planes of thienyl and BBTz group

in **BBTz-X** (ca. 30°), qualitatively consistent with the differences seen in the crystal structures of molecules containing these cores described above. The angles between the plane of the core and that of the adjacent dithenosiloles (which, in both cases, are more-or-less coplanar with the other rings of the "**X**" side arm) are also larger for **BDT-X** (8°) than for **BBTz-X** (3°). The reduced twist angles for **BBTz-X** may allow stronger intermolecular interactions and contribute to the poorer solubility and higher melting temperature referred to above for this compound.

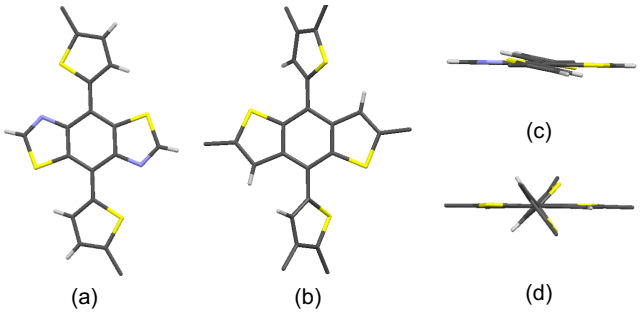

Figure 4. Views showing the 4,8-dithienyl-BBTz and BDT cores in the X-ray structures of (a,c) 4,8-bis(5-(2-ethylhexyl)thiophen-2-yl)benzo[1,2-*d*:4,5-*d'*]bis(thiazole) (see SI) and (b,d) of an intermediate-sized derivative of the BDT core[14] (alkyl substituents and, in the latter case, rhodanine-terminated oligothiophene substituents in the 2,6-positions truncated to single carbon atoms for clarity), respectively, emphasizing the different twist angles between the thienyl groups and the core.

The frontier molecular orbitals (DFT, B3LYP/6-311G*, Figure S3) exhibit subtle differences between the two molecules. In both cases the HOMO extends over the core and the rings of the "X" side-arms, but the HOMO coefficients on the 4,8-dithienyl substituents of **BBTz-X** are greater than those on the corresponding rings of **BDT-X**, consistent with the reduced twist angle in the former compound. The HOMO energy is lower for **BBTz-X** than for **BDT-X**, consistent with the presence of more electronegative atoms in the core of the former. The LUMOs are, in both cases, primarily localized on the thiadiazolopyridine moiety, but somewhat greater coefficients are observed on the core for **BBTz-X** than for **BDT-X**, presumably due to both the greater coplanarity with the side-arms and the electronegativity of N. Consistent with the localization of the LUMO on the acceptor groups of the side arms, the LUMO energy, although still somewhat lower for **BBTz-X**, is less sensitive to the choice of core than the HOMO energy, leading to a larger fundamental (HOMO–LUMO) gap for **BBTz-X** than for **BDT-X**. These findings are fully consistent with the electrochemical and (assuming that the lowest lying excited state can be well-described as a HOMO–LUMO transition) optical data.

Molecular Organization in the Solid State. The molecular order of **BDT-X** and **BBTz-X** in neat thin films was investigated using grazing incidence wide-angle X-ray scattering (GIWAXS). The effects of different post-deposition treatment conditions, specifically thermal annealing (TA) and solvent vapor annealing (SVA), were also characterized. Films were obtained by heating chloroform solutions (5 mg mL^{-1}) on a 50 °C hot plate for 30 min, after removal from heat and allowing to cool to room temperature, the solution was spin-casted onto Si substrates at 2000 rpm without filtration, followed by TA at 100 °C for 10 min or SVA in tetrahydrofuran (THF) for 1 min. Figure 5 and Figure S4 show the GIWAXS images, while out-of-plane and in-plane linecuts are summarized in Figure S5. As-cast films of **BDT-X** and **BBTz-X** are very similar to one another; both show a strong in-plane reflection at q = 0.33 $Å^{-1}$ (d = 19 Å) and an out-of-plane reflection at q = 1.74 $Å^{-1}$ (d = 3.6 Å), which we attribute to the lateral repeat distance (parallel to the molecular plane and perpendicular to the long axis of the molecules) dictated by the alkyl chains and to π-π stacking, respectively, with the molecular planes lying parallel to the substrate ("π-face-on" orientation). The lack of significantly different π-stacking distances between the two compounds might at first appear surprising in view of the less planar molecular structure expected for **BDT-X** (see above), but the previously reported crystal structure of a molecule with a 4,8-dithienyl-BDT core discussed above demonstrates that the out-of-plane 4,8-dithienyl groups do not necessarily disrupt π-stacking; in that previous structure the thienyl substituents do not interfere with those of neighboring molecules due to displacement of adjacent molecules along the long molecular axis, resulting in a small π-stacking distance of 3.64 Å.[14] Thermal or solvent vapor treatments of **BBTz-X** and **BDT-X** neat film lead to negligible change of d-spacing along π-π stacking direction (Table S1). The crystalline correlation length (CCL), a parameter related to characteristic grain size, was deduced for each sample from the full-width-at-half-maximum (FWHM) of the alkyl stacking (100) peak near q = 0.32 $Å^{-1}$; as-cast **BBTz-X** and **BDT-X** exhibit the same CCL (11.2 nm) for the as-cast films, while TA and SVA leads to peak narrowing, corresponding to increased CCL, the most dramatic increase being seen for TA **BDT-X** (CCL = 20.3 nm, Table S1). The crystal orientation distribution can be determined using pole figures (Figure S6 and S7), which plot the diffraction intensity of the peak against the azimuthal angle. The full width at half maximum (FWHM) of the pole figure describes the breadth of the orientation distribution (Table S2). The post-deposition treatments (TA and SVA) for both films lead to narrower distributions of crystal orientation, with the largest effects being observed for alkyl-stacking reflection, and with SVA giving the narrowest distribution of orientations; the FWHM is reduced from 56° and 51° to 37° and 29° after SVA for **BBTz-X** and **BDT-X**, respectively. To summarize, both molecules exhibit π-face-on orientation (in contrast to **X2**, which adopts a predominantly "edge-on" orientation on Si[54]), and the post-deposition treatments can lead to more orientationally ordered crystallites.

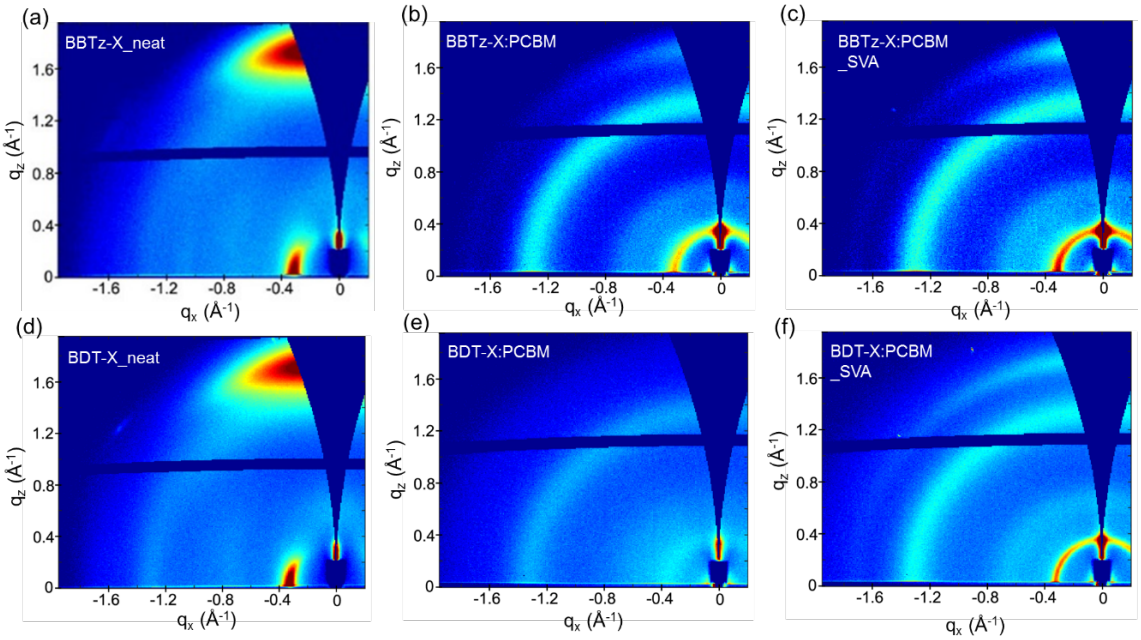

Figure 5. GIWAXS profiles of as-cast neat films of (a) **BBTz-X** and(d) **BDT-X**, as-cast blend films of (b) **BBTz-X**:$PC_{61}BM$ and(e) **BDT-X**:$PC_{61}BM$, and blend films of (e) **BBTz-X**:$PC_{61}BM$ and (f) **BDT-X**:$PC_{61}BM$ after solvent-vapor annealing for 1 min.

Charge-Transport Properties. Bottom-contact-bottom-gate organic field-effect transistors (OFET) were used to investigate the charge-carrier mobility in neat films parallel to the substrate plane (*i.e.*, perpendicular to the π-stacking direction inferred from the GIWAXS data). It should be noted that the OFET devices were not intensively optimized, their primary purpose being to show their potential of these materials as semiconductors, and compare the effects of TA and SVA on charge transport. Solutions in chloroform (5 mg mL^{-1}) were spin-coated onto substrates, consisting of a 300 nm SiO_2 dielectric grown on heavily n-doped Si, with gold source and drain electrodes defining a channel width and length of 2 mm and 50 μm respectively. Transfer curves are shown in Figure 6 (see Figure S13 for thermal stability tests), and the resulting mobilities calculated from the saturation regime are listed in Table S5. Both materials show moderate hole mobility values (μ_h). For the as-cast films, **BDT-X** shows higher μ_h (4.7×10^{-3} $cm^2 V^{-1} s^{-1}$), compared with **BBTz-X** (1.7×10^{-3} $cm^2 V^{-1} s^{-1}$). After TA and SVA, the mobilities increase ca. 2 to 3 times for both molecules, perhaps due to the increased crystallinity revealed by the GIWAXS data. The highest mobility for **BBTz-X** is 4.7×10^{-3} $cm^2 V^{-1} s^{-1}$ after TA at 100 °C, and for **BDT-X** is 1.3×10^{-2} $cm^2 V^{-1} s^{-1}$ upon SVA. Devices with either material show good thermal stability, reflected in μ_h values of 6.6×10^{-4} and 7.4×10^{-3} $cm^2 V^{-1} s^{-1}$ for **BBTz-X** and **BDT-X**, respectively, at 200 °C.

Photovoltaic Performance. The photovoltaic properties of new compounds were investigated with conventional architectures, ITO/MoO_x/donor:$PC_{61}BM$/Ca/Al (donor = **BBTz-X**, **BDT-X**, or **X2**; ITO = indium tin oxide). The MoO_x hole extraction layer was vacuum-deposited, and the active layer were spin-coated from $CHCl_3$ solutions with a total concentration of 20 mg mL^{-1}. Different donor:$PC_{61}BM$ ratios, film thickness, additives, and post-treatment conditions were investigated systematically. Photovoltaic parameters obtained under AM 1.5G at 100 mA cm^{-2} are summarized in Tables S6, S7, and S8 and indicate that the optimal donor:$PC_{61}BM$ weight ratio was ca. 50:50 for both **BBTz-X** and **BDT-X** donors. Parameters for devices with optimized ratio and thickness (see Table S7 for optimization) with different post-deposition treatments are compared in Table 2. TA or SVA of **BDT-X** devices increases the efficiency from ca. 3% to ca. 6% or ca. 8%, respectively, through large increases in the fill factor (*FF*) and moderate increases in the short-circuit current (J_{sc}) more than compensating for a slight decrease in open-circuit voltage (V_{oc}). This enhanced *FF* and J_{sc}, but lower V_{oc} are consistent with other reports of the effects of SVA treatment,[14,55,56] where the solvent vapor is thought to penetrate the film, allowing the molecules to reorganize with more ordered packing. The increased J_{sc} is consistent with EQE measurements (shown in Figure 7), and with stronger absorption seen with *in-situ* UV-vis measurements (Figure S23). It has also previously been shown that SVA can increase μ_h,[56] consistent with what is observed here (see below). As-cast **BBTz-X**:$PC_{61}BM$ blends are much more efficient (ca. 6%) than as-cast **BDT-X**:$PC_{61}BM$ blends, largely due to a much larger *FF*. Partly due to less room for *FF* improvement and less significant J_{sc} enhancement (consistent with EQE, Figure 7, and in-situ UV-vis, Figure S24, measurements), post-deposition treatments do not lead to such dramatic enhancements in efficiency for **BBTz-X**:$PC_{61}BM$ (up to ca. 7% after SVA treatment). The greater solubility of **BDT-X** may also be a factor in the greater sensitivity to SVA found for **BDT-X**:$PC_{61}BM$ devices.

J_{sc} values for the optimized devices are both significantly lower than for devices incorporating the previously reported molecule **X2** (fabricated under the optimized

conditions, performance comparable to that in the literature[14]); this is at least partly attributable to the lower energy absorption onset for **X2** (Table 1). On the other hand, higher V_{oc} and *FF* factors are achievable for the new compounds, the higher V_{OC} values being consistent with the more anodic oxidation potentials and deeper DFT-calculated HOMOs, leading to overall higher efficiencies after SVA. Although it is tempting to also ascribe the differences in V_{oc} between SVA **BBTz-X** and **BDT-X** to differences in redox potential / HOMO energies, it is worth noting that, as shown in Table 2, higher V_{oc} values are obtained in the as-cast devices and are within experimental uncertainty for the two molecules

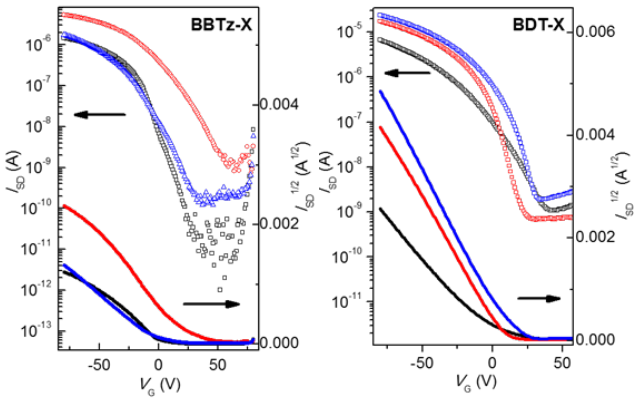

Figure 6. OFET transfer curves for **BBTz-X** and **BDT-X** after spin-coating (black), thermal annealing (blue) and solvent vapor annealing (red).

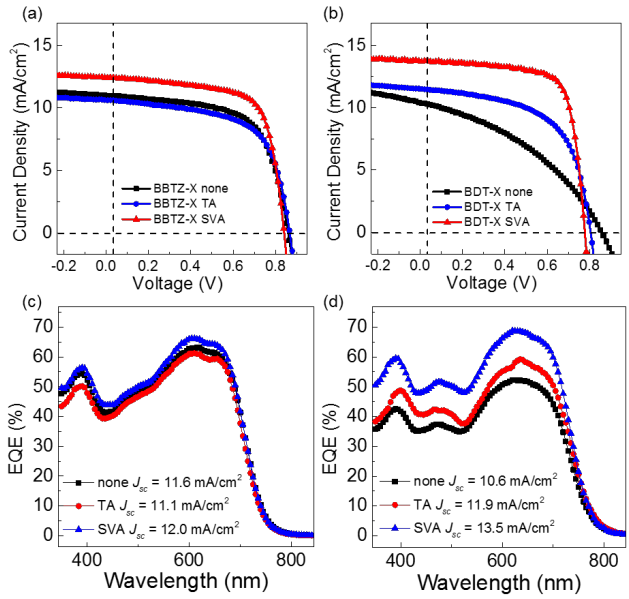

Figure 7. Current–voltage characteristics of molecule:$PC_{61}BM$ BHJ solar cell devices for (a) **BBTz-X** and (b) **BDT-X** under different conditions. EQE curves of the corresponding devices for (c) **BBTz-X** and (d) **BDT-X**.

Table 2. Photovoltaic Parameters for BDT-X, BBTz-X and X2 Fabricated under the Same Conditions.[a,b]

Donor:Acceptor	Film treatment	J_{sc} / mA cm^{-2}	V_{oc} / V	FF / %	η / %	best η / %
	as-cast	11.14 ± 0.25	0.87 ± 0.01	60.04 ± 1.25	6.02 ± 0.23	6.20
BBTz-X:$PC_{61}BM$	TA	11.53 ± 0.21	0.86 ± 0.01	62.78 ± 0.37	6.09 ± 0.19	6.26
	SVA	12.27 ± 0.31	0.84 ± 0.01	69.50 ± 0.44	7.20 ± 0.30	7.39
	as-cast	10.18 ± 0.20	0.86 ± 0.01	38.20 ± 0.62	3.34 ± 0.10	3.47
BDT-X:$PC_{61}BM$	TA	11.85 ± 0.17	0.81 ± 0.01	58.48 ± 0.72	5.51 ± 0.24	5.66
	SVA	13.71 ± 0.21	0.78 ± 0.01	73.04 ± 0.91	7.74 ± 0.31	8.10
	as-cast	15.15 ± 0.47	0.69 ± 0.06	65.21 ± 6.3	6.76 ± 0.17	6.98
X2:$PC_{61}BM$	TA	15.50 ± 0.48	0.68 ± 0.01	59.87 ± 2.26	6.31 ± 0.10	6.39
	SVA	15.41 ± 0.19	0.66 ± 0.01	69.00 ± 1.62	7.01 ± 0.12	7.19

[a]The optimized thickness for **BBTz-X**, **BDT-X**, and **X2** blend films are ca.130 nm, 120 nm and 100 nm, respectively. For all the TA treatments, the blend fims were anealed at 100 °C for 10 min, while for the SVA treatments, the blend films were exposed in tetrahydrofuran (THF) vapor for 1 min. [b]Results are averages and standard deviations for ca. 50 devices for each device type.

J–V characteristics for **BBTz-X** and **BDT-X** BHJ devices were also measured at varying light intensities.[57-59] Plots of J_{sc} vs. light intensity, *I*, were fitted as $J_{SC} \propto I^S$; values of *S* for **BDT-X** devices increase from 0.89 to 0.90 to 0.92 from as-cast to TA to SVA films, suggesting that annealing results in reduced recombination (in the absence of which it is expected that $S = 1$);[57] on the other hand, values of *S* for **BBTz-X** devices are higher (0.94-0.97) and less sensitive to annealing, consistent with the lower sensitivity of other OPV parameters to annealing (Table 2). For all the BHJ films, fitting the intensity dependence of V_{oc} to $V_{oc} = V_o + (nk_BT/e)\ln(I)$, where V_o is a constant and *e* the electronic charge, affords values of *n* close to unity, indicating, as in other OPV cells, that recombination processes are predominantly bimolecular (Figure S17).

The blend films were also investigated by GIWAXS (Figures 3 and S8). For all the blend films, an isotropic ring feature is observed at $q = 1.36$ Å^{-1}, ($d = 4.62$ Å) and is attributed to scattering from amorphous $PC_{61}BM$. Arc-like features at $q = 0.35$ (**BBTz-X**) or 0.36 Å^{-1} (**BDT-X**) are attributed to the lateral alkyl-stacking of the donors; for both molecules, these are seen at somewhat higher *q* (lower *d*-spacing) than the neat film. As in the case of neat films, post-deposition treatments can decrease *q* for this feature; in this case TA having the largest effect in both cases (Table S3 and, for *in-situ* monitoring of the

effect of TA, Figure S12). π-Stacking distances are essentially the same as found in neat films, although the π-stacking was not observed for the as-cast film of **BDT-X**:$PC_{61}BM$. In the BHJ films, there is a broader distribution of molecular orientations, as indicated by pole figures (Figure S10 and S11) than in neat films; as in the neat films, these distributions are generally centered around a π-face-on orientation, although the pole figure for the π-stacking reflection of the TA BBTz-X also has some edge-on orientation (Figure S10). The CCLs (Table S3) for the blend films of both donors follow the order SVA > TA > as-cast.

Atomic force microscopy (AFM) was used to investigate topography and phase separation (Figures S18 and S19) in BHJ spin-coated from chloroform onto substrates consisting of MoO_x (9 nm) vacuum deposited onto ITO-coated glass. The topographic images reveal similar roughness for as-cast BHJ films of both donors and that TA significantly increases the roughness, while SVA does not, although more well-defined fiber-like features are evident for the **BBTz-X**. For both **BBTz-X** and **BDT-X** blends, the size of the fiber-like domains evident in the phase images increase in the order TA > SVA > as-cast films, which do not appear to be correlated with the donor CCL values determined using GIWAXS. However, the top surface microstructure from topographic images does not necessarily correlate with the bulk microstructure from GIWAXS.

SCLC measurements on hole- and electron-only devices were used to quantify the charge-carrier mobilities perpendicular to the substrate plane in the BHJ blend films. μ_h values of 3.4×10^{-4} and 2.5×10^{-4} $cm^2 V^{-1} s^{-1}$ for as-cast BHJ films of **BBTz-X** and **BDT-X**, respectively (Figure S14, Table S5), are obtained, comparable to those reported for other high-efficiency small-/intermediate-molecule BHJ films;[14,15,47] these increase to 5.8×10^{-4} and 3.6×10^{-3} $cm^2 V^{-1} s^{-1}$ after SVA. Electron mobilities (μ_e, Table S5) obtained from electron-only devices vary from 7.0×10^{-5} to 7.0×10^{-4} $cm^2 V^{-1} s^{-1}$; μ_e and μ_e values are fairly well balanced for all **BBTz-X**:$PC_{61}BM$ blends and for SVA **BDT-X**:$PC_{61}BM$ blends, but much less so for as-cast and TA **BDT-X**:$PC_{61}BM$ blends, consistent with the trends seen in FF values (Table 2).[23,54]

CONCLUSION

Two oligomers with different cores, **BBTz-X** and **BDT-X**, were synthesized and characterized. The variation of the core from BDT to BBTz affects optical absorptions, thermal stabilities, molecular geometries, energy levels, film morphology and charge-transport properties for both the pristine donor film and blend films with the $PC_{61}BM$. More planar molecular structures and anodically shifted redox potentials were observed for **BBTz-X** than for **BDT-X**, which lead to much more efficient solar cell devices of as-cast blend films with the former (ca. 6%) than the latter molecule (ca. 3%). Post-deposition annealing treatments allow the molecules to reorganize with more ordered packing, and lead to remarkable enhancements in efficiency for **BDT-X**:$PC_{61}BM$ mostly through large increases in the fill factor (*FF*), but are less effective in **BBTz-X** blend films. From **BDT-X** to **BBTz-X**, the V_{oc} increased from 0.78 eV to 0.84 eV, while the J_{sc} and *FF* decreased slightly. Higher efficiency was demonstrated with BDT-X (avg. 7.7%) than BBTz-X (avg. 7.2%)

ASSOCIATED CONTENT

Supporting Information

The Supporting Information is available free of charge on the ACS Publications website.

Experimental details for synthesis, characterization, OPV work, and crystal-structure determination; figures showing TGA, DSC, GIWAXS, OFET, SCLC, OPV, AFM, *in-situ* UV-vis., and single-crystal X-ray data; and NMR spectra of new compounds (PDF)

Crystallographic data for 4,8-bis(5-(2-ethylhexyl)thiophen-2-yl)-benzo[1,2-d:4,5-d']bis(thiazole) (CIF)

AUTHOR INFORMATION

Corresponding Author

* E-mail: seth.marder@chemistry.gatech.edu.

ORCID

Timothy C. Parker: 0000-0002-0270-0364
Tatiana V. Timofeeva: 0000-0001-7475-3206
Aram Amassian: 0000-0002-5734-1194
Guillermo C. Bazan: 0000-0002-2537-0310
Simon B. Blakey: 0000-0002-4100-8610
Stephen Barlow: 0000-0001-9059-9974
Seth R. Marder: 0000-0001-6921-2536

Author Contributions

‡S.Z. and J.Z. contributed equally to the work.

Notes

The authors declare no competing financial interest.

ACKNOWLEDGMENT

The research was partly supported by the National Science Foundation, through the CCI Center for Selective C–H Functionalization (CHE-1205646 and CHE-1700982) and through the PREM program (DMR-1523611), and by the Department of the Navy, Office of Naval Research, through Award No. N00014-14-1-0580 (CAOP MURI).

REFERENCES

(1) Lin, Y.; Zhan, X. Non-Fullerene Acceptors for Organic Photovoltaics: An Emerging Horizon. *Mater. Horiz.* **2014**, *1*, 470-488.

(2) Ala'a, F. E.; Sun, J.-P.; Hill, I. G.; Welch, G. C. Recent Advances of Non-Fullerene, Small Molecular Acceptors for Solution Processed Bulk Heterojunction Solar Cells. *J. Mater. Chem. A* **2014**, *2*, 1201-1213.

(3) Dou, L.; Liu, Y.; Hong, Z.; Gang Li; Yang, Y. Low-Bandgap near-Ir Conjugated Polymers/Molecules for Organic Electronics. *Chem. Rev.* **2015**, *115*, 12633–12665.

(4) Ni, W.; Wan, X.; Li, M.; Wang, Y.; Chen, Y. A–D–a Small Molecules for Solution-Processed Organic Photovoltaic Cells. *Chem. Commun.* **2015**, *51*, 4936-4950.

(5) Liu, C.; Wang, K.; Gong, X.; Heeger, A. J. Low Bandgap Semiconducting Polymers for Polymeric Photovoltaics. *Chem. Soc. Rev.* **2016**, *45*, 4825-4846.

(6) Jung, J. W.; Jo, J. W.; Jung, E. H.; Jo, W. H. Recent Progress in High Efficiency Polymer Solar Cells by Rational Design and Energy Level Tuning of Low Bandgap Copolymers with Various Electron-Withdrawing Units. *Org. Electron.* **2016**, *31*, 149–170.

(7) Benten, H.; Mori, D.; Ohkita, H.; Ito, S. Recent Research Progress of Polymer Donor/Polymer Acceptor Blend Solar Cells. *J. Mater. Chem. A* **2016**, *4*, 5340-5365.

(8) Kang, H.; Lee, W.; Oh, J.; Kim, T.; Lee, C.; Kim, B. J. From Fullerene–Polymer to All-Polymer Solar Cells: The Importance of Molecular Packing, Orientation, and Morphology Control. *Acc. Chem. Res.* **2016**, *49*, 2424-2434.

(9) Ostroverkhova, O. Organic Optoelectronic Materials: Mechanisms and Applications. *Chem. Rev.* **2016**, *116*, 13279–13412.

(10) Xiao, S.; Zhang, Q.; You, W. Molecular Engineering of Conjugated Polymers for Solar Cells: An Updated Report. *Adv. Mater.* **2017**, 1601391.

(11) Zhao, J.; Li, Y.; Yang, G.; Jiang, K.; Lin, H.; Ade, H.; Ma, W.; Yan, H. Efficient Organic Solar Cells Processed from Hydrocarbon Solvents. *Nat. Energy* **2016**, *1*, 15027.

(12) Zhao, W.; Li, S.; Yao, H.; Zhang, S.; Zhang, Y.; Yang, B.; Hou, J. Molecular Optimization Enables over 13% Efficiency in Organic Solar Cells. *J. Am. Chem. Soc.* **2017**, *139*, 7148–7151.

(13) Kan, B.; Li, M.; Zhang, Q.; Liu, F.; Wan, X.; Wang, Y.; Ni, W.; Long, G.; Yang, X.; Feng, H.; Zuo, Y.; Zhang, M.; Huang, F.; Cao, Y.; Russell, T. P.; Chen, Y. A Series of Simple Oligomer-Like Small Molecules Based on Oligothiophenes for Solution-Processed Solar Cells with High Efficiency. *J. Am. Chem. Soc.* **2015**, *137*, 3886-3893.

(14) Sun, K.; Xiao, Z.; Lu, S.; Zajaczkowski, W.; Pisula, W.; Hanssen, E.; White, J. M.; Williamson, R. M.; Subbiah, J.; Ouyang, J.; Holmes, A. B.; Wong, W. W. H.; Jones, D. J. A Molecular Nematic Liquid Crystalline Material for High-Performance Organic Photovoltaics. *Nat. Commun.* **2015**, *6*, 6013.

(15) Bin, H.; Yang, Y.; Zhang, Z.-G.; Ye, L.; Ghasemi, M.; Chen, S.; Zhang, Y.; Zhang, C.; Sun, C.; Xue, L.; Yang, C.; Ade, H.; Li, Y. 9.73% Efficiency Nonfullerene All Organic Small Molecule Solar Cells with Absorption-Complementary Donor and Acceptor. *J. Am. Chem. Soc.* **2017**, *139*, 5085-5094.

(16) Walker, B.; Kim, C.; Nguyen, T.-Q. Small Molecule Solution-Processed Bulk Heterojunction Solar Cells. *Chem. Mater.* **2011**, *23*, 470-482.

(17) Shang, H.; Fan, H.; Liu, Y.; Hu, W.; Li, Y.; Zhan, X. A Solution-Processable Star-Shaped Molecule for High-Performance Organic Solar Cells. *Adv. Mater.* **2011**, *23*, 1554-1557.

(18) Lee, O. P.; Yiu, A. T.; Beaujuge, P. M.; Woo, C. H.; Holcombe, T. W.; Millstone, J. E.; Douglas, J. D.; Chen, M. S.; Fréchet, J. M. J. Efficient Small Molecule Bulk Heterojunction Solar Cells with High Fill Factors Via Pyrene-Directed Molecular Self-Assembly. *Adv. Mater.* **2011**, *23*, 5359-5363.

(19) Lin, Y.; Li, Y.; Zhan, X. Small Molecule Semiconductors for High-Efficiency Organic Photovoltaics. *Chem. Soc. Rev.* **2012**, *41*, 4245-4272.

(20) Liu, Y.; Yang, Y.; Chen, C.-C.; Chen, Q.; Dou, L.; Hong, Z.; Li, G.; Yang, Y. Solution-Processed Small Molecules Using Different Electron Linkers for High-Performance Solar Cells. *Adv. Mater.* **2013**, *25*, 4657–4662.

(21) Sun, Y.; Welch, G. C.; Leong, W. L.; Takacs, C. J.; Bazan, G. C.; Heeger, A. J. Solution-Processed Small-Molecule Solar Cells with 6.7% Efficiency. *Nat. Mater.* **2012**, *11*, 44.

(22) Zhou, J.; Wan, X.; Liu, Y.; Zuo, Y.; Li, Z.; He, G.; Long, G.; Ni, W.; Li, C.; Su, X.; Chen, Y. Small Molecules Based on Benzo[1,2-*b*:4,5-*b*′]Dithiophene Unit for High-Performance Solution-Processed Organic Solar Cells. *J. Am. Chem. Soc.* **2012**, *134*, 16345-16351.

(23) Liu, X.; Sun, Y.; Hsu, B. B. Y.; Lorbach, A.; Qi, L.; Heeger, A. J.; Bazan, G. C. Design and Properties of Intermediate-Sized Narrow Band-Gap Conjugated Molecules Relevant to Solution-Processed Organic Solar Cells. *J. Am. Chem. Soc.* **2014**, *136*, 5697-5708.

(24) Zhou, J.; Zuo, Y.; Wan, X.; Long, G.; Zhang, Q.; Ni, W.; Liu, Y.; Li, Z.; He, G.; Li, C.; Kan, B.; Li, M.; Chen, Y. Solution-Processed and High-Performance Organic Solar Cells Using Small Molecules with a Benzodithiophene Unit. *J. Am. Chem. Soc.* **2013**, *135*, 8484-8487.

(25) Yao, H.; Ye, L.; Zhang, H.; Li, S.; Zhang, S.; Hou, J. Molecular Design of Benzodithiophene-Based Organic Photovoltaic Materials. *Chem. Rev.* **2016**, *116*, 7397-7457.

(26) Lin, Y.; Zhan, X. Oligomer Molecules for Efficient Organic Photovoltaics. *Acc. Chem. Res.* **2016**, *49*, 175–183.

(27) Abdelsamie, M.; Treat, N. D.; Zhao, K.; McDowell, C.; Burgers, M. A.; Li, R.; Smilgies, D. M.; Stingelin, N.; Bazan, G. C.; Amassian, A. Toward Additive-Free Small-Molecule Organic Solar Cells: Roles of the Donor Crystallization Pathway and Dynamics. *Adv. Mater.* **2015**, *27*, 7285-7292.

(28) Lin, Y.; Ma, L.; Li, Y.; Liu, Y.; Zhu, D.; Zhan, X. A Solution-Processable Small Molecule Based on Benzodithiophene and Diketopyrrolopyrrole for High-Performance Organic Solar Cells. *Adv. Energy Mater.* **2013**, *3*, 1166-1170.

(29) Lin, Y.; Ma, L.; Li, Y.; Liu, Y.; Zhu, D.; Zhan, X. Small-Molecule Solar Cells with Fill Factors up to 0.75 Via a Layer-by-Layer Solution Process. *Adv. Energy Mater.* **2014**, *4*, 1300626.

(30) Sun, K.; Xiao, Z.; Lu, S.; Zajaczkowski, W.; Pisula, W.; Hanssen, E.; White, J. M.; Williamson, R. M.; Subbiah, J.; Ouyang, J.; Holmes, A. B.; Wong, W. W. H.; Jones, D. J. A Molecular Nematic Liquid Crystalline Material for High-Performance Organic Photovoltaics. *Nat. Commun.* **2015**, *6*.

(31) Subbiah, J.; Purushothaman, B.; Chen, M.; Qin, T.; Gao, M.; Vak, D.; Scholes, F. H.; Chen, X.; Watkins, S. E.; Wilson, G. J.; Holmes, A. B.; Wong, W. W.; Jones, D. J. Organic Solar Cells Using a High-Molecular- Weight Benzodithiophene-Benzothiadiazole Copolymer with an Efficiency of 9.4%. *Adv. Mater.* **2015**, *27*, 702-705.

(32) Wang, J.; Shi, K.; Suo, Y.; Lin, Y.; Yu, G.; Zhan, X. Monodisperse Macromolecules Based on Benzodithiophene and Diketopyrrolopyrrole with Strong NIR Absorption and High Mobility. *J. Mater. Chem. C* **2016**, *4*, 3781-3791.

(33) Lin, Y.; Wang, J.; Li, T.; Wu, Y.; Wang, C.; Han, L.; Yao, Y.; Ma, W.; Zhan, X. Efficient Fullerene-Free Organic Solar Cells Based on Fused-Ring Oligomer Molecules. *J. Mater. Chem. A* **2016**, *4*, 1486-1494.

(34) Xu, Z.; Fan, Q.; Meng, X.; Guo, X.; Su, W.; Ma, W.; Zhang, M.; Li, Y. Selenium-Containing Medium Bandgap Copolymer for Bulk Heterojunction Polymer Solar Cells with High Efficiency of 9.8%. *Chem. Mater.* **2017**, *29*, 4811-4818.

(35) Eastham, N. D.; Dudnik, A. S.; Harutyunyan, B.; Aldrich, T. J.; Leonardi, M. J.; Manley, E. F.; Butler, M. R.; Harschneck, T.; Ratner, M. A.; Chen, L. X.; Bedzyk, M. J.; Melkonyan, F. S.; Facchetti, A.; Chang, R. P. H.; Marks, T. J. Enhanced Light Absorption in Fluorinated Ternary Small-Molecule Photovoltaics. *ACS Energy Lett.* **2017**, *2*, 1690-1697.

(36) Yu, R.; Zhang, S.; Yao, H.; Guo, B.; Li, S.; Zhang, H.; Zhang, M.; Hou, J. Two Well-Miscible Acceptors Work as One for Efficient Fullerene-Free Organic Solar Cells. *Adv. Mater.* **2017**, *29*, 1700437.

(37) Tam, T. L. D.; Lin, T. T. Tuning Energy Levels and Film Morphology in Benzodithiophene–Thienopyrrolodione

Copolymers via Nitrogen Substitutions. *Macromolecules* **2016**, *49*, 1648-1654.

(38) Zhao, W.; Li, S.; Zhang, S.; Liu, X.; Hou, J. Ternary Polymer Solar Cells Based on Two Acceptors and One Donor for Achieving 12.2% Efficiency. *Adv. Mater.* **2016**, *29*, 1604059.

(39) Ahmed, E.; Kim, F. S.; Xin, H.; Jenekhe, S. A. Benzobisthiazole-Thiophene Copolymer Semiconductors: Synthesis, Enhanced Stability, Field-Effect Transistors, and Efficient Solar Cells. *Macromolecules* **2009**, *42*, 8615-8618.

(40) Ahmed, E.; Subramaniyan, S.; Kim, F. S.; Xin, H.; Jenekhe, S. A. Benzobisthiazole-Based Donor Acceptor Copolymer Semiconductors for Photovoltaic Cells and Highly Stable Field-Effect Transistors. *Macromolecules* **2011**, *44*, 7207.

(41) Bhuwalka, A.; Mike, J. F.; He, M.; Intemann, J. J.; Nelson, T.; Ewan, M. D.; Roggers, R. A.; Lin, Z.; Jeffries-EL, M. Quaterthiophene Benzobisazole Copolymers for Photovoltaic Cells: Effect of Heteroatom Placement and Substitution on the Optical and Electronic Properties. *Macromolecules* **2011**, *44*, 9611.

(42) Wakayima, A.; Hagiya, K.; Hamamoto, S.; Tanaka, H. World Patent Application: 2015; WO/2015/060183.

(43) Bon, J. L.; Feng, D.; Marder, S. R.; Blakey, S. B. A C–H Functionalization Protocol for the Direct Synthesis of Benzobisthiazole Derivatives. *J. Org. Chem.* **2014**, *79*, 7766-7771.

(44) Shi, Q.; Zhang, S.; Zhang, J.; Oswald, V. F.; Amassian, A.; Marder, S. R.; Blakey, S. B. Kotbu-Initiated Aryl C–H Iodination: A Powerful Tool for the Synthesis of High Electron Affinity Compounds. *J. Am. Chem. Soc.* **2016**, *138*, 3946-3949.

(45) Huo, L.; Zhang, S.; Guo, X.; Xu, F.; Li, Y.; Hou, J. Replacing Alkoxy Groups with Alkylthienyl Groups: A Feasible Approach to Improve the Properties of Photovoltaic Polymers. *Angew. Chem. Int. Ed.* **2011**, *50*, 9697-9702.

(46) Ye, L.; Zhang, S.; Huo, L.; Zhang, M.; Hou, J. Molecular Design toward Highly Efficient Photovoltaic Polymers Based on Two-Dimensional Conjugated Benzodithiophene. *Acc. Chem. Res.* **2014**, *47*, 1595-1603.

(47) Oosterhout, S. D.; Savikhin, V.; Zhang, J.; Zhang, Y.; Burgers, M. A.; Marder, S. R.; Bazan, G. C.; Toney, M. F. On the Mixing Behavior in Small Molecule:Fullerene Organic Photovoltaics. *Chem. Mater.* **2017**, **,** *29*, 3062-3069.

(48) Homyak, P. D.; Tinkham, J.; Lahti, P. M.; Coughlin, E. B. Thieno [3,4-*b*] Thiophene Acceptors with Alkyl, Aryl, Perfluoroalkyl, and Perfluorophenyl Pendants for Donor–Acceptor Low Bandgap Polymers. *Macromolecules* **2013**, *46*, 8873-8881.

(49) Mugesh, G.; Singh, H. B.; Butcher, R. J. Non-Bonded S...N Interactions in Organosulfur Derivatives: Crystal and Molecular Structures of [2-(4,4-Dimethyl-2-oxazolinyl)phenyl]benzyl Sulfide and Bis[2-(4,4-dimethyl-2-oxazolinyl)phenyl]sulfide. *J. Chem. Res. S* **1999**, 472-473.

(50) Lin, S.; Wrobleski, S. T.; Hynes Jr, J.; Pitt, S.; Zhang, R.; Fan, Y.; Doweyko, A. M.; Kish, K. F.; Sack, J. S.; Malley, M. F.; Kiefer, S. E.; Newitt, J. A.; McKinnon, M.; Trzaskos, J.; Barrish, J. C.; Dodd, J. H.; Schieven, G. L.; Leftheris, K. Utilization of a Nitrogen–Sulfur Nonbonding Interaction in the Design of New 2-Aminothiazol-5-yl-pyrimidines as P38α Map Kinase Inhibitors. *Bioorg. Med. Chem. Lett.* **2010**, *20*, 5864-5868.

(51) Hayashi, K.; Ogawa, S.; Sano, S.; Shiro, M.; Yamaguchi, K.; Sei, Y.; Nagao, Y. Intramolecular Nonbonded S–N Interaction in Rabeprazole. *Chem. Pharm. Bull.* **2008**, *56*, 802-806.

(52) Fukumoto, S.; Nakashima, T.; Kawai, T. Photon-Quantitative Reaction of a Dithiazolylarylene in Solution. *Angew. Chem., Int. Ed.* **2011**, *50*, 1565-1568.

(53) Beno, B. R.; Yeung, K.-S.; Bartberger, M. D.; Pennington, L. D.; Meanwell, N. A. A Survey of the Role of Noncovalent Sulfur Interactions in Drug Design. *J. Med. Chem.* **2015**, *58*, 4383-4438.

(54) Liu, X.; Sun, Y.; Perez, L. A.; Wen, W.; Toney, M. F.; Heeger, A. J.; Bazan, G. C. Narrow-Band-Gap Conjugated Chromophores with Extended Molecular Lengths. *J. Am. Chem. Soc.* **2012**, *134*, 20609-20612.

(55) He, Z.; Zhong, C.; Huang, X.; Wong, W. Y.; Wu, H.; Chen, L.; Su, S.; Cao, Y. Simultaneous Enhancement of Open-Circuit Voltage, Short-Circuit Current Density, and Fill Factor in Polymer Solar Cells. *Adv. Mater.* **2011**, *23*, 4636-4643.

(56) Sun, K.; Xiao, Z.; Hanssen, E.; Klein, M. F.; Dam, H. H.; Pfaff, M.; Gerthsen, D.; Wong, W. W.; Jones, D. J. The Role of Solvent Vapor Annealing in Highly Efficient Air-Processed Small Molecule Solar Cells. *J. Mater. Chem. A* **2014**, *2*, 9048-9054.

(57) Lu, L.; Xu, T.; Chen, W.; Landry, E. S.; Yu, L. Ternary Blend Polymer Solar Cells with Enhanced Power Conversion Efficiency. *Nature Photonics* **2014**, *8*, 716-722.

(58) Cowan, S. R.; Roy, A.; Heeger, A. J. Recombination in Polymer-Fullerene Bulk Heterojunction Solar Cells. *Phys. Rev. B* **2010**, *82*, 245207.

(59) Koster, L. J. A.; Kemerink, M.; Wienk, M. M.; Maturová, K.; Janssen, R. A. J. Quantifying Bimolecular Recombination Losses in Organic Bulk Heterojunction Solar Cells. *Adv. Mater.* **2011**, *23*, 1670-1674.

.

For Table of Contents: